BJR

https://doi.org/10.1259/bjr.20190757

Received: 03 September 2019 | Revised: 26 November 2019 | Accepted: 27 December 2019

Cite this article as:
Kim E, Kim CK, Kim HS, Jang DP, Kim IY, Hwang J. Histogram analysis from stretched exponential model on diffusion-weighted imaging: evaluation of clinically significant prostate cancer. *Br J Radiol* 2020; **93**: 20190757.

FULL PAPER

Histogram analysis from stretched exponential model on diffusion-weighted imaging: evaluation of clinically significant prostate cancer

[1,2]EUNJU KIM, PhD, [3,4,5]CHAN KYO KIM, MD, [6]HYUN SOO KIM, MD, [1]DONG PYO JANG, PhD, [1]IN YOUNG KIM, MD, PhD and [2]JINWOO HWANG, MS

[1]Department of Biomedical Engineering, Hanyang University, Seoul, Republic of Korea
[2]Philips Healthcare, Seoul, Republic of Korea
[3]Department of Radiology and Center for Imaging Science, Samsung Medical Center, Sungkyunkwan University School of Medicine, Seoul, Republic of Korea
[4]Department of Medical Device Management and Research, SAIHST Sungkyunkwan University, Seoul, Republic of Korea
[5]Department of Digital Health, SAIHST, Sungkyunkwan University, Seoul, Republic of Korea
[6]Department of Medicine, Graduate School, Kyung Hee University, Seoul, Republic of Korea

Address correspondence to: Dr Chan Kyo Kim
E-mail: *chankyokim@skku.edu*

The authors Chan Kyo Kim and Dong Pyo Jang contributed equally to the work.

Objective: To evaluate the usefulness of histogram analysis of stretched exponential model (SEM) on diffusion-weighted imaging in evaluating clinically significant prostate cancer (CSC).
Methods: A total of 85 patients with prostate cancer underwent 3T multiparametric MRI, followed by radical prostatectomy. Histogram parameters of the tumor from the SEM [distributed diffusion coefficient (DDC) and α] and the monoexponential model [MEM; apparent diffusion coefficient (ADC)] were evaluated. The associations between parameters and Gleason score or Prostate Imaging Reporting and Data System v. 2 were evaluated. The area under the receiver operating characteristics curve was calculated to evaluate diagnostic performance of parameters in predicting CSC.
Results: The values of histogram parameters of DDC and ADC were significantly lower in patients with CSC than in patients without CSC ($p < 0.05$), except for skewness and kurtosis. The value of the 25th percentile of α was significantly lower in patients with CSC than in patients without CSC ($p = 0.014$). Histogram parameters of ADC and DDC had significant weak to moderate negative associations with Gleason score or Prostate Imaging Reporting and Data System v. 2 ($p < 0.001$), except for skewness and kurtosis. For predicting CSC, the area under the curves of mean ADC (0.856), 50th percentile DDC (0.852), and 25th percentile α (0.707) yielded the highest values compared to other histogram parameters from each group.
Conclusion: Histogram analysis of the SEM on diffusion-weighted imaging may be a useful quantitative tool for evaluating CSC. However, the SEM did not outperform the MEM.
Advances in knowledge: Histogram parameters of SEM may be useful for evaluating CSC.

INTRODUCTION

Prostate cancer (PCa) is one of the most common causes of cancer-related death in males worldwide.[1] The current standard tool in diagnosing PCa is transrectal ultrasound-guided biopsy. However, it has limitations including a false-negative rate (47%),[2] the underestimation of the Gleason score (GS) in 34–46% of cases,[3] and the overdiagnosis and overtreatment of indolent disease.[4] Prostate multiparametric MRI (mpMRI) has increasingly been used for the detection and risk stratification of clinically significant cancer (CSC).

Recently, in 2015, the Prostate Imaging Reporting and Data System (PI-RADS) version 2 (v. 2) was introduced to standardize the image acquisition technique and interpretation of prostate mpMRI.[5] In PI-RADS v. 2 guidelines, diffusion-weighted imaging (DWI) and apparent diffusion coefficient (ADC) map are the dominant sequences in the peripheral zone of the prostate and it is recommended that a monoexponential model (MEM) to be used to obtain ADC measurements of the signal decay data at different b values (0, 50–100, and 800–1000 s/mm^2).[5] However, clear scientific evidence supporting this recommendation is still lacking.

With advances in MR hardware and software, the use of higher *b* values (>1000 s/mm^2), advanced DWI acquisition and modeling methods have been possible.[6] Non-Gaussian behavior of diffusion reflects tissue heterogeneity and irregularity, which can be demonstrated using high *b*-value DWI and requires advanced DWI modeling.[6–9] The stretched exponential model (SEM) can reflect the deviation of the curve from monoexponential behavior.[10–12] The SEM DWI has been applied to malignant tumors, such as brain, kidney, cervix, and ovary tumors.[13–17] Only a few studies have demonstrated that SEM DWI could be useful in assessing PCa aggressiveness and for detecting PCa.[6,9,11,12] However, few studies have reported the results following the evaluation of PCa using histogram analysis of SEM DWI.[11] This method requires more validation in order to be adopted in the clinical practice. Therefore, the purpose of this study was to evaluate the value of histogram analysis of SEM DWI in evaluating CSC.

METHODS AND MATERIALS

Subjects

Our local institutional review board approved the study and waived the need for informed consent because of the retrospective study design. Between September 2015 and January 2016, 106 patients with biopsy-proven PCa who underwent prostate mpMRI received radical prostatectomy. These patients fulfilled the following inclusion criteria: 1) pre-operative mpMRI including DWI at 3 T and 2) no prior radiation therapy, chemotherapy or hormonal therapy. Of these, 21 males were excluded: outside MRI (n = 17) and several DWI artifacts (n = 4). Finally, 85 consecutive males (mean age, 67.1 years; range, 44–81 years) were included in this study (Figure 1). The mean time interval between MRI examination and surgery was 51.7 days. The locations of cancers were as follows: peripheral zone (n = 56), transition zone (n = 24), and both (n = 5).

Figure 1. Flow chart of patient enrollment. CSC,clinically significant cancer; DWI, diffusion-weighted imaging.

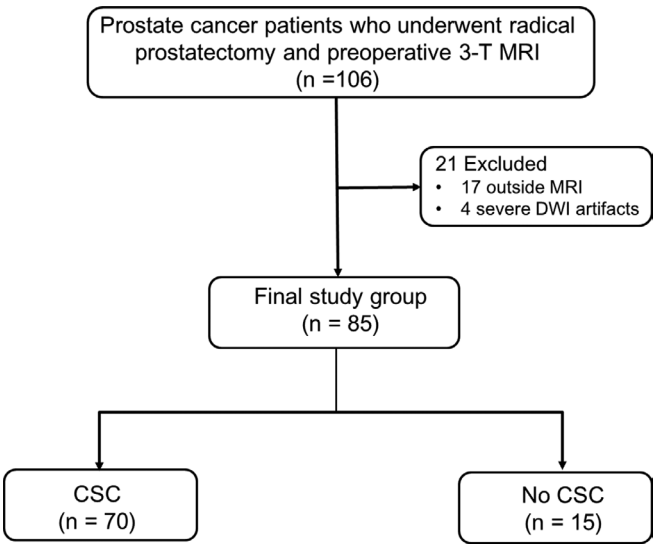

MRI protocols

MRI examinations were performed using a 3 T MRI scanner (Achieva TX, Philips Healthcare, Best, The Netherlands) equipped with a phased-array coil. The routine MRI protocols included T_2 weighted, T_1 weighted, DWI and dynamic contrast-enhanced imaging according to the PI-RADS v. 2 guidelines.[5]

T_2 weighted turbo spin echo images of axial, coronal and sagittal planes were obtained using the following imaging parameters: repetition time (TR)/echo time (TE), 3800–4700/80–100 ms; slice thickness, 3 mm; interslice gap, 1 mm; matrix, 568 × 341; field of view (FOV), 20 cm; number of signals acquired (NSA), 3; sensitivity encoding (SENSE) factor, 2; and number of slices, 21. Axial DWI was obtained using the single-shot echo planar imaging technique with the following parameters: TR/TE, 4400–4800/63–75 ms; slice thickness, 3 mm; interslice gap, 1 mm; matrix, 112 × 112–110; FOV, 20 cm; SENSE factor 2; NSA, 4; number of slices, 20; and *b*–values, 0, 100, 1000 and 1500 s/mm^2. Axial dynamic contrast-enhancing imaging was obtained using a three-dimensional (3D)-fast field echo sequence [TR/TE, 7.4/3.9 ms; flip angle, 5° and 15° (pre-contrast) and 25° (post-contrast); matrix, 224 × 179; slice thickness, 4 mm; interslice gap, no; NSA, 1; FOV, 20 cm; and 11 partitions on a 3D slab]. The 3D volume with 11 partitions was acquired every 3 s with 60 repetitions. A post-contrast image was obtained immediately after a bolus injection of gadolinium-based contrast agents at a dose of 0.1 mmol/kg body weight and a rate of 2–3 ml s^{-1} using a power injector and a 20 ml saline flush was followed.

Image and histologic analysis

All MR images were reviewed by an experienced genitourinary radiologist (C.K.K., with 13 years of experience in prostate MRI) who was blinded to the clinical results of each patient to minimize the bias, but was aware of pathological findings.

Quantitative analyses of histogram parameters were performed using diffusion analysis software (EXPRESS; Philips Healthcare, Korea) based on MEM and SEM.[10,18,19] For analysis of images acquired from high-*b*-value DWI, parametric maps were developed by fitting the following models to the pixel signal intensity (SI) at the different *b* values, as follows.

For the MEM DWI,

S/S0 = exp (-bADC), where S represents the SI at a particular *b*-value, S0 is the estimated SI at b = 0 s/mm^2, and the ADC acquired from monoexponential fit.

For the SEM DWI,

S/S0 = exp (-bDDC)$^{\alpha}$, where S represents the SI at a particular *b*-value, and S0 is the SI for a b = 0 s/mm^2 image. The distributed diffusion coefficient (DDC) is a measure of the rate of signal decay with various *b* values, representing mean intravoxel diffusion rates. The index α is the water molecular diffusion heterogeneity and related to intravoxel water diffusion heterogeneity (range, 0–1). A higher α value indicates low intravoxel diffusion heterogeneity, which approaches pure monoexponential decay. The α

Figure 2. 67-year-old male with a left peripheral zone cancer (arrow) with a PSA of 12.9 ng ml^{-1}, size of 1.8 cm, and a GS of 4 + 3=7. (A-B, Axial T_2-weighted image shows a heterogeneous hypointense lesion in the left peripheral zone (arrow), with focal extracapsular extension. On the diffusion-weighted image with b = 1500 s/mm^2 (B), the tumor shows marked hyperintensity (arrow). The PI-RADS v. 2 score is 5. (C-E) Axial ADC (C), DDC (D) and α (E) maps including all histograms. The mean values of the ADC, DDC, and α in the tumor (region of interest) are 624.8 × 10^{-6} mm^2/s, 897.9 × 10^{-6} mm^2/s, and 0.731, respectively. ADC,apparent diffusion coefficient; DDC, distributed diffusion coefficient; PI-RADS,Prostate Imaging Reporting and Data System.

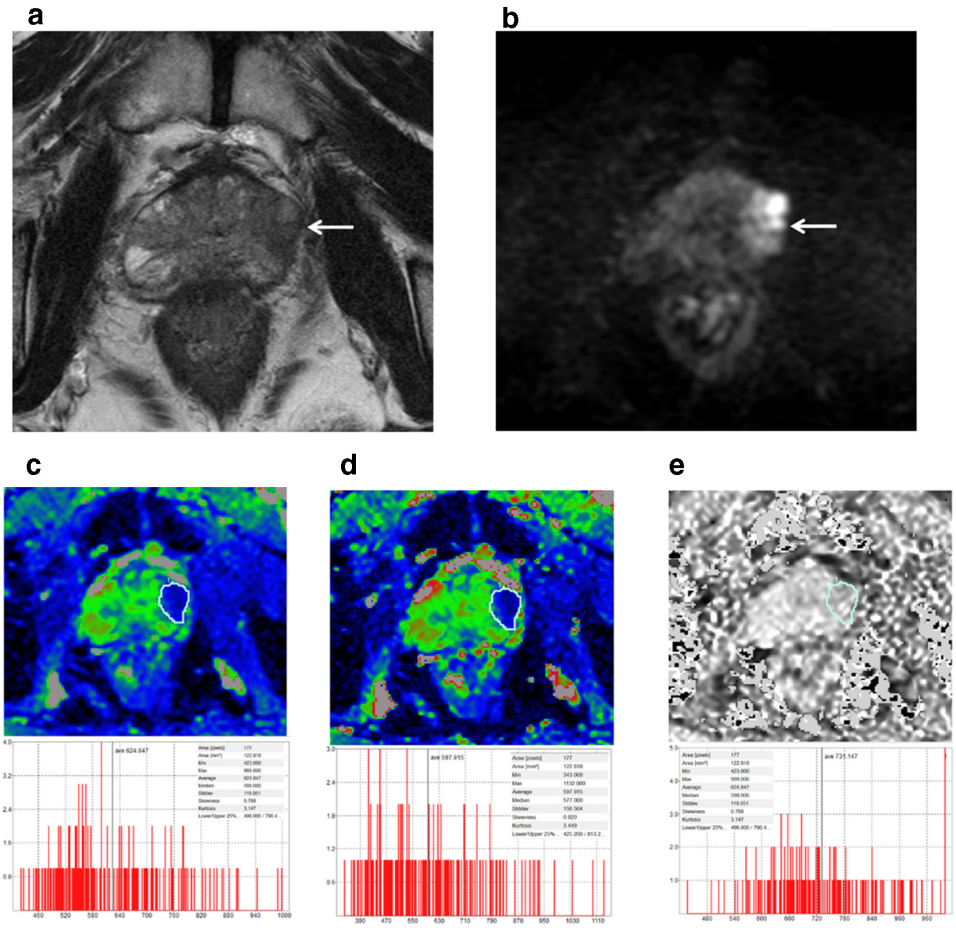

= 1 is equivalent to monoexponential diffusion-weighted signal decay (*i.e.* low intravoxel diffusion heterogeneity). Conversely, an α = 0 indicates a higher degree of multiexponential signal decay.[14] The DDC is biexponential estimates of diffusion rates on the time allowed for diffusion and not directly reflect the fluid viscosity unless diffusion is unrestricted.

Regions of interest (ROIs) were manually drawn around the entire visible tumor on the ADC maps: each ROI in each ADC map of a tumor focus were summed to obtain voxel-by-voxel values for histogram analysis. However, it did not include edge voxels to avoid a partial volume effect. The ROIs on ADC maps were copied onto the corresponding areas on either the DDC or α map (Figure 2). In cases without visible tumors on ADC maps, the ROI measurements were performed in the areas where tumors were identified on the histopathological findings. The histogram parameters of ADC, DDC and α values were minimum (ADC_{min}, DDC_{min}, and α_{min}), 25th percentile (ADC25, DDC25, and α25), 50th percentile (ADC50, DDC50, and α50), 75th percentile (ADC75, DDC75, and α75), maximum (ADC_{max}, DDC_{max}, and α_{max}), mean (ADC_{mean}, DDC_{mean}, and α_{mean}), skewness ($ADC_{skewness}$, $DDC_{skewness}$, and $\alpha_{skewness}$) and kurtosis ($ADC_{kurtosis}$, $DDC_{kurtosis}$, and $\alpha_{kurtosis}$). In addition, to evaluate interobserver reliability and variability of histogram parameters, a less-experienced radiologist (H.S.K., with 1 year of experience in prostate MRI) manually drew the ROIs in the tumors for 20 patients in the same manner as the first measurement. The quantitative values were measured twice at the same site and the average was recorded.

More than 4 weeks after the end of quantitative analysis, qualitative analysis was performed by a radiologist (C.K.K.) according to the PI-RADS v. 2 guidelines for assessing the likelihood of CSC.[5] The PI-RADS score per patient for an index tumor using a 5-point scale was recorded. The index tumor was considered when a tumor was seen on mpMRI with the highest PI-RADS score. If the highest PI-RADS score assigned to the tumors were ≥2, one that shows extracapsular extension or is larger was considered as the index tumor. The greatest axial diameter of the index tumor was also recorded in accordance with the strategy for lesion measurement of the PI-RADS v. 2. Tumors with a GS ≥3 + 4 were considered to be CSC.

The histopathological findings in a whole-mounted step section of the prostate were used as the standard reference. An experienced pathologist who was blinded to the MRI findings reviewed all slides prepared from the tissue slices. Tumor size and volume, distribution, extracapsular extension, seminal vesicle invasion, lymph node metastasis, and GS were reported.

Statistical analysis

The patients were classified into two groups: the group with CSC and the group without CSC. Continuous parameters were compared using the Student *t*-test or Mann–Whitney test, and categorical data were compared using Fisher's exact test or χ^2 test. As clinical parameters, age, prostate specific antigen (PSA), PSA density, prostate volume, and digital rectal examination (DRE) findings were included. Spearman rank correlation was used to evaluate the associations between parameters and GS or PI-RADS v. 2 scoring.

To evaluate diagnostic performance and identify optimal cut-off values for the prediction of CSC, receiver operating characteristics (ROC) curve analysis was used and the area under the curve (AUC), sensitivity, and specificity were also calculated. The Youden index was calculated to identify the optimal cut-off value of each parameter for the prediction of CSC. Of clinical or imaging parameters, parameters that showed significant association with GS were evaluated at ROC curve analysis.

Interobserver reliability and variability were evaluated using an intraclass correlation coefficient (ICC) and an Altman–Bland plot, respectively. Reliability, assessed using the ICC value, was considered to be poor when the ICC value was between 0.00 and 0.20, fair when the ICC value was between 0.21 and 0.40, moderate when the ICC value was between 0.41 and 0.60, good when the ICC value was between 0.61 and 0.80, and excellent when the ICC value was between 0.81 and 1.00. All statistical analysis was performed using SPSS software (v. 23.0, SPSS, Chicago, IL) and Medcalc (v. 13.0; MedCalc Software, Mariakerke, Belgium).Two-sided p values < 0.05 were considered statistically significant.

RESULT

Clinical characteristics

The clinical characteristics are presented in Table 1. At histopathological findings, CSC was found in 70 patients (82.4%), while clinically insignificant cancer was found in the remaining

Table 1. Clinical characteristics

Parameter	All (n = 85)	CSC (-) (n = 15)	CSC (+) (n = 70)	p-value*
Age (year)	67.1 (44–81)	66.4 (57–78)	67.2 (44–81)	0.507
PSA (ng/ml)	10.7 (1.7–54.7)	6.2 (1.9–14.1)	11.7 (1.7–54.7)	0.034
Prostate volume (cm^3)	35.9 (11–101)	41.2 (18–101)	34.8 (11–100)	0.493
PSA density ($ng/ml/cm^3$)	0.33 (0.07–1.45)	0.17 (0.07–0.41)	0.37 (0.07–1.47)	0.007
Tumor size (mm)	16.6 (0–45)	9.5 (0–13.7)	18.1 (0–45)	<0.001
DRE (+)	21	1	20	0.017
PI-RADS v. 2				<0.001
2	4 (4.7)	2 (13.3)	2 (2.9)	
3	4 (4.7)	3 (20.0)	1 (1.4)	
4	35 (41.2)	10 (66.7)	25 (35.7)	
5	42 (49.4)	0 (0)	42 (60.0)	
Surgical findings				
Tumor volume (cm^3)	5.15 (0.03–81.80)	0.45 (0.03–2.50)	6.15 (0.30–81.80)	<0.001
Gleason score				na
6	15 (17.6)	15 (100.0)	0	
3 + 4	35 (41.2)	0	35 (50.0)	
4 + 3	18 (21.2)	0	18 (25.7)	
8	8 (9.4)	0	8 (11.4)	
9	9 (10.6)	0	9 (12.9)	
Extracapsular extension (+)	34	0	34	<0.001
Seminal vesicle invasion (+)	8	0	8	0.340

CSC, clinically significant cancer; DRE, digital rectal examination; PI-RADS, Prostate Imaging Reporting and Data System; PSA, prostate specific antigen.

Data are presented as mean (range) or n (%).

[a]Statistical differences between the two groups.

Table 2. Histogram parameters of the monoexponential and stretched-exponential DWI models

Parameter	All (n = 85)	CSC (-) (n = 15)	CSC (+) (n = 70)	p-value[a]
ADC histogram ($\times 10^{-6}$ mm^2/s)				
ADC_{mean}	795 ± 271	1100 ± 416	729 ± 171	<0.001
ADC_{min}	633 ± 234	880 ± 344	580 ± 163	<0.001
ADC25	686 ± 240	941 ± 361	631 ± 164	<0.001
ADC50	798 ± 319	1088 ± 426	719 ± 173	<0.001
ADC75	912 ± 302	1258 ± 470	838 ± 187	<0.001
ADC_{max}	1008 ± 314	1337 ± 471	937 ± 215	<0.001
$ADC_{skewness}$	0.37 ± 0.73	0.14 ± 0.75	0.41 ± 0.72	0.19
$ADC_{kurtosis}$	3.22 ± 1.74	2.79 ± 0.82	3.31 ± 1.87	0.291
DDC histogram ($\times 10^{-6}$ mm^2/s)				
DDC_{mean}	819 ± 323	1188 ± 449	740 ± 224	<0.001
DDC_{min}	604 ± 277	900 ± 391	541 ± 199	<0.001
DDC25	658 ± 285	982 ± 408	588 ± 195	<0.001
DDC50	798 ± 319	1158 ± 450	721 ± 221	<0.001
DDC75	970 ± 397	1404 ± 514	876 ± 298	<0.001
DDC_{max}	1287 ± 1623	1538 ± 552	1233 ± 1768	0.041
$DDC_{skewness}$	254 ± 220	0.15 ± 0.72	309 ± 2420	0.624
$DDC_{kurtosis}$	4.89 ± 9.75	2.90 ± 0.86	5.31 ± 10.71	0.388
DDC_{mean}	819 ± 323	1188 ± .449	740 ± 224	<0.001
α histogram				
α_{mean}	0.760 ± 0.074	0.788 ± 0.092	0.754 ± 0.069	0.1
α_{min}	0.656 ± 0.670	0.626 ± 0.126	0.663 ± 0.737	0.848
α25	0.629 ± 0.087	0.678 ± 0.111	0.618 ± 0.077	0.014
α50	0.747 ± 0.083	0.775 ± 0.092	0.741 ± 0.078	0.152
α75	0.901 ± 0.077	0.904 ± 0.077	0.900 ± 0.078	0.858
α_{max}	0.968 ± 0.056	0.957 ± 0.065	0.970 ± 0.054	0.416
$\alpha_{skewness}$ ($\times 10^{-3}$)	4.32 ± 38.49	0.19 ± 0.61	5.29 ± 42.41	0.644
$\alpha_{kurtosis}$ ($\times 10^{-3}$)	2.58 ± 0.93	2.66 ± 0.81	2.56 ± 0.96	0.714

ADC, apparent diffusion coefficient; CSC, clinically significant cancer; DDC, distributed diffusion coefficient..
Data are presented as mean ± standard deviation.
[a]Statistical differences between the two groups.

15 patients (17.6%). The values of the PSA, PSA density, tumor size on MRI, and tumor volume were significantly higher in the group with CSC than in the group without CSC (all-p <0.05). The group with CSC had a significantly higher PI-RADS v 2 score than the group without CSC (p < 0.001). The group with CSC had significantly higher proportion of palpable nodule on digital rectal examination or extracapsular extension as compared with the group without CSC (p = 0.007 and p < 0.001, respectively). No significant differences were found between the groups regarding age, prostate volume, and seminal vesical invasion (all-p >0.05).

Histogram parameters of monoexponential and stretched exponential DWI

Table 2 presents the results for histogram parameters of the MEM and SEM between the groups with and without CSC. In the MEM, all ADC parameters for the group with CSC were significantly lower than those for the group without CSC (all-p <0.001), except for skewness (p = 0.190) and kurtosis (p = 0.291). In the SEM, all DDC parameters for the group with CSC were significantly lower in the group with CSC than those for the group without CSC (all-p <0.001), except for skewness (p =

0.624) and kurtosis (p = 0.388). Among the α histogram parameters, only α50 was significantly different between the groups (p = 0.014).

Associations between parameters and GS or PI-RADS v. 2

The associations between histogram parameters and GS or PI-RADS v. 2 are presented in Table 3. Regarding associations with the GS, all ADC parameters, except for skewness and kurtosis, had significantly moderate negative associations (ρ = −0.411 to −0.470) (all-p <0.001). With the exception of skewness and kurtosis, all DDC parameters showed significantly negatively either moderate (DDC_{mean}, DDC_{min}, DDC25, DDC50 and DDC75; ρ = −0.428 to −0.466) or weak (DDC_{max}; ρ = −0.376) associations (all-p <0.001). Among the α parameters, only α_{min} and α25 showed significantly negative weak associations (ρ = −0.289, p = 0.007; ρ = −0.217, p = 0.041).

Regarding associations with PI-RADS v. 2, all ADC and DDC parameters showed significantly weak to moderate negative associations (ρ = −0.388 to −0.428; ρ = −0.308 to −0.419; all-p <0.01), except for skewness and kurtosis. Among the α parameters, only α_{min} and α25 showed significantly weak negative association (ρ = −0.259, p = 0.017; ρ = −0.231, p = 0.047).

Of clinical parameters, tumor size (ρ = 0.419, p < 0.001) and PI-RADS v. 2 (ρ = 0.504, p < 0.001) showed significantly moderate positive associations with the GS. The PSA density (ρ = 0.296, p = 0.006) and PSA (ρ = 0.231, p = 0.033) had significantly weak associations with the GS. However, age, DRE and prostate volume had no significant association with the GS (all-p >0.05).

ROC curve analysis

Table 4 presents the diagnostic performance and optimal cutoff for the prediction of CSC. The AUCs of all parameters for the DDC (0.785–0.852) were similar to those of the corresponding parameters for the ADC (0.811–0.856) (all-p <0.05). The AUCs of α25 and α_{min} were 0.707 and 0.703, respectively. Among the clinical parameters, PI-RADS v. 2 had the highest AUC (0.843) followed by tumor size (AUC = 0.817).

For the prediction of CSC, the AUCs of ADC_{mean} (0.856), DDC50 (0.852), and α25 (0.707) that showed the highest values compared to other histogram parameters of each group were not significant different with that of PI-RADS v 2 in pairwise comparisons: PI-RADS v. 2 *vs* ADC_{mean}, p = 0.821; PI-RADS v 2 *vs* DDC50, p = 0.874; PI-RADS v 2 *vs* α25, p = 0.149).

Interobserver reliability and variability

Interobserver reliability of all ADC and DDC parameters were excellent (ICC = 0.893–0.953 for ADC; ICC = 0.874–0.937 for DDC), except for $ADC_{skewness}$ (ICC = 0.620), $ADC_{kurtosis}$ (ICC = 0.245), $DDC_{skewness}$ (ICC = 0.002), and $DDC_{kurtosis}$ (ICC = 0.504). Interobserver reliability of α parameters was good to excellent (ICC = 0.6172–0.824), with the exception of those for $\alpha_{skewness}$ (ICC = 0.146) and $\alpha_{kurtosis}$ (ICC = −0.405). For the interobserver variability in the Altman–Bland plots, the mean differences of ADC parameters ranged from 0.4 to 11.3%,

Table 3. Association of histogram parameters from the DWI models with the Gleason score and PI-RADS v. 2

Histogram parameter	Gleason score						PI-RADS v. 2					
	ADC		DDC		α		ADC		DDC		α	
	ρ	*p*-value	ρ	*p*-value	ρ	*p*-value	ρ	*p*-value	ρ	*p*-value	ρ	*p*-value
Mean	−0.470	<0.001	−0.466	<0.001	−0.207	0.057	−0.428	<0.001	−0.419	<0.001	−0.128	0.245
Minimum	−0.421	<0.001	−0.428	<0.001	−0.289	0.007	−0.401	<0.001	−0.36	0.001	−0.259	0.017
25th percentile	−0.436	<0.001	−0.452	<0.001	−0.217	0.041	−0.412	<0.001	−0.308	0.004	−0.231	0.047
Median	−0.466	<0.001	−0.465	<0.001	−0.155	0.156	−0.419	<0.001	_0.419	<0.001	−0.076	0.487
75th percentile	−0.463	<0.001	−0.444	<0.001	−0.019	0.865	−0.413	<0.001	−0.314	0.003	−0.013	0.916
Maximum	−0.411	<0.001	−0.376	<0.001	0.197	0.071	−0.388	<0.001	−0.349	0.001	0.154	0.159
Skewness	0.108	0.327	0.158	0.147	−0.019	0.861	0.126	0.252	0.201	0.065	−0.075	0.497
Kurtosis	0.108	0.324	0.083	0.45	−0.02	0.859	0.007	0.953	−0.091	0.407	−0.11	0.317

ADC, apparent diffusion coefficient; DDC, distributed diffusion coefficient; PI-RADS, Prostate Imaging Reporting and Data System.

Table 4. Diagnostic performance of imaging and clinical parameters for the prediction of CSC

Parameter	AUC	Cutoff	Sensitivity (%)	Specificity (%)	*p*-value
ADC histogram ($\times10^{-6}$ mm^2/s)					
ADC_{mean}	0.856	≤797	68.6	93.3	<0.001
ADC_{min}	0.819	≤827	94.3	60	<0.001
ADC25	0.830	≤848	94.3	60	<0.001
ADC50	0.853	≤803	72.9	86.7	<0.001
ADC75	0.851	≤994	78.6	86.7	<0.001
ADC_{max}	0.811	≤1086	75.7	86.7	<0.001
DDC histogram ($\times10^{-6}$ mm^2/s)					
DDC_{mean}	0.849	≤840	71.4	93.3	<0.001
DDC_{min}	0.824	≤838	94.3	60	<0.001
DDC25	0.842	≤640	62.9	93.3	<0.001
DDC50	0.852	≤830	72.9	86.7	<0.001
DDC75	0.836	≤1049	74.3	86.7	<0.001
DDC_{max}	0.785	≤1150	68.6	86.7	<0.001
α histogram					
α_{min}	0.703	≤0.590	67.1	73.3	0.0183
α25	0.707	≤0.637	61.4	80	0.0210
Clinical					
PSA	0.675	>5.47	72.9	66.7	0.0236
DRE	0.643	palpable	28.6	100	<0.001
Tumor size	0.817	>13.7	64.3	100	<0.001
PI-RADS v. 2	0.843	5	60	100	<0.001
PSA density	0.723	>0.158	71.4	73.3	0.0011

ADC, apparent diffusion coefficient; DDC, distributed diffusion coefficient; DRE, digital rectal examination; PI-RADS, Prostate Imaging Reporting and Data System; PSA, prostate-specific antigen.

except that for skewness (230.4%). The mean differences of DDC parameters ranged from 0.9 to 12.6%, except that for skewness (53.8%). The mean differences of α parameters ranged from 0.1 to 10.7%, except that for skewness (76.1%).

DISCUSSION

The mpMRI is the best imaging tool for detecting and staging PCa and DWI is an essential sequence of mpMRI.[5] To date, many studies have investigated deviations in the diffusion signal from monoexponential behavior using high *b*-value DWI.[8,9,11,12,19] Complex parametric models considered from high *b*-value DWI include the bi-exponential model, diffusion kurtosis imaging and SEM. The SEM was first introduced by Bennett et al[10] to evaluate diffusion and intravoxel heterogeneity, as represented by the parameters of DDC and α. Several recent studies have demonstrated the potential of the SEM for detecting PCa or tumor aggressiveness.[6,9,11,12] However, other studies have reported that MEM DWI alone may be sufficient in evaluating PCa in clinical practice.[8,20] Accordingly, further studies remain to be investigated for clinical usefulness of the SEM as compared with the MEM.

Risk stratification is very crucial for patient counseling and for the selection of optimal treatment strategies because PCa has heterogeneous behaviors.[21] In this study, we found that the values of DDC parameters from SEM DWI were significantly lower in the group with CSC than in the group without CSC. In the ROC curve analysis, these DDC parameters had good diagnostic performance for predicting CSC (AUC = 0.785–0.852). However, these results of the DDC parameters were not significantly different from those of the ADC parameters. These findings suggest that the SEM did not outperform the MEM in evaluating CSC. Thus, we believe that the MEM alone may be sufficient in clinical practice. Further studies on this subject are needed.

The histogram analysis has several advantages. It provides statistical information and offers a quantitative methodology for analyzing nonsignificant changes in the pixels of tumors.[22] The percentiles may be useful in evaluating malignant components of lesions through the identification of different microenvironments that may be masked by mean ADC values. In addition, changes in the shape of the histogram and the degree of asymmetry indicated by kurtosis and skewness can reflect changes

in microstructures. To date, only a recent study by Liu et al[11] has reported the potential usefulness of histogram analysis of DDC and ADC parameters in differentiating low GS from high GS cancers. Consistent with the previous study,[11] our results demonstrated that histogram parameters of DDC and ADC were significantly different between groups with and without CSC.

The Gleason grading system has consistently demonstrated a prognostic value in PCa patients.[23] The ADC from MEM is a known marker for assessing PCa aggressiveness.[24,25] In the present study, ADC and DDC parameters showed significantly negative associations with the GS, which is consistent with the findings of a previous study.[11] Of these ADC or DDC parameters, ADC_{mean} and DDC_{50} showed the highest associations with GS ($\rho = -0.470$ and -0.466, respectively).

The mpMRI including T_2 weighted imaging, DWI and dynamic contrast-enhanced imaging is associated with tumor GS.[26] Several studies have reported that the PI-RADS v. 2 could provide excellent diagnostic accuracy for CSC detection, with 82–89% sensitivity and 72–73% specificity.[27,28] Although PI-RADS v. 2 does not provide quantitative information, it reflects tumor aggressiveness because a higher score in the prostate indicates hypointensity on ADC map with markedly hyperintense on DWI. In the present study, DDC parameters showed weak to moderate associations with the PI-RADS v. 2 scores and the values of DDC parameters were equivalent to those of ADC parameters. These results were consistent with those of previous studies.[29]

The α value is used to describe the deviation of water diffusion.[10,12] A few studies reported that α values are not associated with the GS in PCa.[6,11] However, our study demonstrated that α_{min} and α25 value have weak negative associations with the GS or PI-RADS v. 2. Moreover, the AUCs of α_{min} and α25 were 0.703 and 0.707 for predicting CSC, respectively. These findings suggest that the α value might have somewhat potential for evaluating tumor heterogeneity or assessing tumor aggressiveness. However, these findings seem to be insufficient to be used in clinical practice. Additionally, PCa aggressiveness may be dependent on tissue architecture including the luminal, epithelial, and stromal components and changes in PCa aggressiveness may be dependent on the size of the PCa and not only on the tumor heterogeneity.[30]

The skewness and kurtosis may be strong and quantitative predictors of tumor heterogeneity.[31] However, our results showed that the skewness and kurtosis from MEM and SEM are not associated with the GS or PI-RADS v. 2 and are not significantly different between groups with and without CSC. Our results are consistent with those of a previous study[11] that demonstrated no significant correlation with GS. These findings may be explained that GS in PCa is based on tissue microscopic features including epithelial, luminal and stromal components, and its change is based on their relative sizes rather than only tumor heterogeneity.[30] Thus, further investigations are needed.

In the ROC curve analysis of our study, the ADC_{mean} and DDC50 had the highest AUC for predicting CSC compared to other histogram parameters for each group. Although SEM DWI can offer useful information for diffusion and intravoxel heterogeneity, parameters from SEM DWI did not outperform of ADC_{mean} from MEM DWI to predict CSC. Contrary to our results, a recent study reported that the 10th percentile of the ADC and DDC had the highest AUC for differentiating between low and high GS cancers compared to other histogram parameters for each group.[11] Further studies to determine which DDC and ADC histogram parameter is the best for predicting CSC are needed. Interestingly, the ADC_{min}, DDC50, and α25 that had the highest AUC for predicting CSC compared to other histogram parameters for each group had similar AUC with PI-RADS v. 2 at ROC curve analysis. These findings may support the recent updated PI-RADS v. 2.1 that does not include quantitative information on MR sequences.[32] However, a further larger study is warranted.

The reliability and variability of quantitative MRI parameters are essential when these parameters are being considered as potential imaging biomarkers. Our results demonstrated that interobserver agreement for ADC and DDC parameters, except for skewness and kurtosis, were excellent. This finding is consistent with that of a previous study.[19] The interobserver agreement of α parameters, except for skewness and kurtosis, was good to excellent. Interobserver variabilities in all MEM and SEM parameters, except for skewness, were less than 12.6%. Thus, SEM histogram parameters could be used as imaging markers similar to MEM ADC parameters, except for skewness or kurtosis. For poor interobserver agreement and variability for skewness or kurtosis, one potential explanation may be that it is too dependent on microvariation in the ROI placements. However, to increase the use of these parameters in clinical practice, sophisticated software or standardized ROI measurements for tumors will be needed to improve reliability between observers.

Several limitations are worth noting in our study. First, our study was a retrospective study that all included patients received radical prostatectomy in a single institution, indicating a selection bias. Thus, our results may not be translated into other scenarios such as active surveillance or prebiopsy MRI cohorts with elevated PSA. Second, quantitative ROI measurements might contain inevitable errors due to potential radiological-pathological mismatching. Finally, multiexponential diffusion attenuation could be more significant when the *b*-value is high (≥3000 mm^2/s). However, the highest *b*-value in our study was 1500 mm^2/s due to limited signal-to-ratio. A further study is needed.

In conclusion, our results demonstrate that histogram analysis of the SEM on DWI may be a useful quantitative tool for evaluating CSC. However, the SEM did not outperform the MEM.

ACKNOWLEDGMENT

We thank Insuk Sohn, PhD of Statistics and Data Center, Samsung Medical Center, for help with statistical assistance and thank Editage (www.editage.co.kr) for English language editing.

CONFLICT OF INTEREST

The authors report no conflict of interest concerning the materials or methods used in this study or the findings specified in this paper.

REFERENCES

1. Siegel RL, Miller KD, Jemal A, statistics C. *CA Cancer J Clin* 2019; **2019**: 7–34.
2. Taira AV, Merrick GS, Galbreath RW, Andreini H, Taubenslag W, Curtis R, et al. Performance of transperineal template-guided mapping biopsy in detecting prostate cancer in the initial and repeat biopsy setting. *Prostate Cancer Prostatic Dis* 2010; **13**: 71–7. doi: https://doi.org/10.1038/pcan.2009.42
3. Noguchi M, Stamey TA, McNeal JE, Yemoto CM. Relationship between systematic biopsies and histological features of 222 radical prostatectomy specimens: lack of prediction of tumor significance for men with nonpalpable prostate cancer. *J Urol* 2001; **166**: 104–10. doi: https://doi.org/10.1016/S0022-5347(05)66086-7
4. Loeb S, Bjurlin MA, Nicholson J, Tammela TL, Penson DF, Carter HB, et al. Overdiagnosis and overtreatment of prostate cancer. *Eur Urol* 2014; **65**: 1046–55. doi: https://doi.org/10.1016/j.eururo.2013.12.062
5. Weinreb JC, Barentsz JO, Choyke PL, Cornud F, Haider MA, Macura KJ, et al. PI-RADS Prostate Imaging - Reporting and Data System: 2015, Version 2. *Eur Urol* 2016; **69**: 16–40. doi: https://doi.org/10.1016/j.eururo.2015.08.052
6. Toivonen J, Merisaari H, Pesola M, Taimen P, Boström PJ, Pahikkala T, et al. Mathematical models for diffusion-weighted imaging of prostate cancer using b values up to 2000 s/mm(2) : correlation with Gleason score and repeatability of region of interest analysis. *Magn Reson Med* 2015; **74**: 1116–24. doi: https://doi.org/10.1002/mrm.25482
7. Rosenkrantz AB, Padhani AR, Chenevert TL, Koh D-M, De Keyzer F, Taouli B, et al. Body diffusion kurtosis imaging: basic principles, applications, and considerations for clinical practice. *J Magn Reson Imaging* 2015; **42**: 1190–202. doi: https://doi.org/10.1002/jmri.24985
8. Mazaheri Y, Hötker AM, Shukla-Dave A, Akin O, Hricak H. Model selection for high b-value diffusion-weighted MRI of the prostate. *Magn Reson Imaging* 2018; **46**: 21–7. doi: https://doi.org/10.1016/j.mri.2017.10.003
9. Hectors SJ, Semaan S, Song C, Lewis S, Haines GK, Tewari A, et al. Advanced diffusion-weighted imaging modeling for prostate cancer characterization: correlation with quantitative histopathologic tumor tissue Composition-A hypothesis-generating study. *Radiology* 2018; **286**: 918–28. doi: https://doi.org/10.1148/radiol.2017170904
10. Bennett KM, Schmainda KM, Bennett RT, Rowe DB, Lu H, Hyde JS. Characterization of continuously distributed cortical water diffusion rates with a stretched-exponential model. *Magn Reson Med* 2003; **50**: 727–34. doi: https://doi.org/10.1002/mrm.10581
11. Liu W, Liu XH, Tang W, Gao HB, Zhou BN, Zhou LP. Histogram analysis of stretched-exponential and monoexponential diffusion-weighted imaging models for distinguishing low and intermediate/high Gleason scores in prostate carcinoma. *J Magn Reson Imaging* 2018; **48**: 491–8. doi: https://doi.org/10.1002/jmri.25958
12. Liu X, Zhou L, Peng W, Wang H, Zhang Y. Comparison of stretched-Exponential and monoexponential model diffusion-weighted imaging in prostate cancer and normal tissues. *J Magn Reson Imaging* 2015; **42**: 1078–85. doi: https://doi.org/10.1002/jmri.24872
13. Zhang J, Suo S, Liu G, Zhang S, Zhao Z, Xu J, et al. Comparison of Monoexponential, biexponential, Stretched-Exponential, and Kurtosis models of diffusion-weighted imaging in differentiation of renal solid masses. *Korean J Radiol* 2019; **20**: 791–800. doi: https://doi.org/10.3348/kjr.2018.0474
14. Bai Y, Lin Y, Tian J, Shi D, Cheng J, Haacke EM, et al. Grading of gliomas by using Monoexponential, biexponential, and stretched exponential diffusion-weighted MR imaging and diffusion Kurtosis MR imaging. *Radiology* 2016; **278**: 496–504. doi: https://doi.org/10.1148/radiol.2015142173
15. Winfield JM, deSouza NM, Priest AN, Wakefield JC, Hodgkin C, Freeman S, et al. Modelling DW-MRI data from primary and metastatic ovarian tumours. *Eur Radiol* 2015; **25**: 2033–40. doi: https://doi.org/10.1007/s00330-014-3573-3
16. Lin M, Yu X, Chen Y, Ouyang H, Wu B, Zheng D, et al. Contribution of mono-exponential, bi-exponential and stretched exponential model-based diffusion-weighted MR imaging in the diagnosis and differentiation of uterine cervical carcinoma. *Eur Radiol* 2017; **27**: 2400–10. doi: https://doi.org/10.1007/s00330-016-4596-8
17. Li H, Liang L, Li A, Hu Y, Hu D, Li Z, et al. Monoexponential, biexponential, and stretched exponential diffusion-weighted imaging models: quantitative biomarkers for differentiating renal clear cell carcinoma and minimal fat angiomyolipoma. *J Magn Reson Imaging* 2017; **46**: 240–7. doi: https://doi.org/10.1002/jmri.25524
18. Bennett KM, Hyde JS, Schmainda KM. Water diffusion heterogeneity index in the human brain is insensitive to the orientation of applied magnetic field gradients. *Magn Reson Med* 2006; **56**: 235–9. doi: https://doi.org/10.1002/mrm.20960
19. Merisaari H, Toivonen J, Pesola M, Taimen P, Boström PJ, Pahikkala T, et al. Diffusion-Weighted imaging of prostate cancer: effect of b-value distribution on repeatability and cancer characterization. *Magn Reson Imaging* 2015; **33**: 1212–8. doi: https://doi.org/10.1016/j.mri.2015.07.004
20. Jambor I, Merisaari H, Taimen P, Boström P, Minn H, Pesola M, et al. Evaluation of different mathematical models for diffusion-weighted imaging of normal prostate and prostate cancer using high b-values: a repeatability study. *Magn Reson Med* 2015; **73**: 1988–98. doi: https://doi.org/10.1002/mrm.25323
21. Mottet N, Bellmunt J, Bolla M, Briers E, Cumberbatch MG, De Santis M, et al. EAU-ESTRO-SIOG guidelines on prostate cancer. Part 1: screening, diagnosis, and local treatment with curative intent. *Eur Urol* 2017; **71**: 618–29. doi: https://doi.org/10.1016/j.eururo.2016.08.003
22. Zhang W, Zhou Y, Xu X-Q, Kong L-Y, Xu H, Yu T-F, et al. A Whole-Tumor histogram analysis of apparent diffusion coefficient maps for differentiating thymic carcinoma from lymphoma. *Korean J Radiol* 2018; **19**: 358–65. doi: https://doi.org/10.3348/kjr.2018.19.2.358
23. Ham WS, Chalfin HJ, Feng Z, Trock BJ, Epstein JI, Cheung C, et al. New prostate cancer grading system predicts long-term survival following surgery for Gleason score 8-10 prostate cancer. *Eur Urol* 2017; **71**: 907–12. doi: https://doi.org/10.1016/j.eururo.2016.11.006
24. Hambrock T, Somford DM, Huisman HJ, van Oort IM, Witjes JA, Hulsbergen-van de Kaa CA, et al.

Relationship between apparent diffusion coefficients at 3.0-T MR imaging and Gleason grade in peripheral zone prostate cancer. *Radiology* 2011; **259**: 453–61. doi: https://doi.org/10.1148/radiol.11091409

25. Kim R, Kim CK, Park JJ, Kim JH, Seo SI, Jeon SS, et al. Prognostic significance for long-term outcomes following radical prostatectomy in men with prostate cancer: evaluation with prostate imaging reporting and data system version 2. *Korean J Radiol* 2019; **20**: 256–64. doi: https://doi.org/10.3348/kjr.2018.0613
26. Hoeks CMA, Barentsz JO, Hambrock T, Yakar D, Somford DM, Heijmink SWTPJ, et al. Prostate cancer: multiparametric MR imaging for detection, localization, and staging. *Radiology* 2011; **261**: 46–66. doi: https://doi.org/10.1148/radiol.11091822
27. Woo S, Suh CH, Kim SY, Cho JY, Kim SH. Diagnostic performance of prostate imaging reporting and data system version 2 for detection of prostate cancer: a systematic review and diagnostic meta-analysis. *Eur Urol* 2017; **72**: 177–88. doi: https://doi.org/10.1016/j.eururo.2017.01.042
28. Hamoen EHJ, de Rooij M, Witjes JA, Barentsz JO, Rovers MM. Use of the prostate imaging reporting and data system (PI-RADS) for prostate cancer detection with multiparametric magnetic resonance imaging: a diagnostic meta-analysis. *Eur Urol* 2015; **67**: 1112–21. doi: https://doi.org/10.1016/j.eururo.2014.10.033
29. Yim JH, Kim CK, Kim J-H. Clinically insignificant prostate cancer suitable for active surveillance according to prostate cancer research International: active surveillance criteria: utility of PI-RADS V2. *J Magn Reson Imaging* 2018; **47**: 1072–9. doi: https://doi.org/10.1002/jmri.25856
30. Borren A, Moman MR, Groenendaal G, Boeken Kruger AE, van Diest PJ, van der Groep P, et al. Why prostate tumour delineation based on apparent diffusion coefficient is challenging: an exploration of the tissue microanatomy. *Acta Oncol* 2013; **52**: 1629–36. doi: https://doi.org/10.3109/0284186X.2013.787164
31. Just N. Improving tumour heterogeneity MRI assessment with histograms. *Br J Cancer* 2014; **111**: 2205–13. doi: https://doi.org/10.1038/bjc.2014.512
32. Turkbey B, Rosenkrantz AB, Haider MA, Padhani AR, Villeirs G, Macura KJ, et al. Prostate imaging reporting and data system version 2.1: 2019 update of prostate imaging reporting and data system version 2. *Eur Urol* 2019; **76**: 340–51. doi: https://doi.org/10.1016/j.eururo.2019.02.033